Cyclic nucleotide specific phosphodiesterases as potential drug targets for anti-Leishmania therapy

Cyclic nucleotide specific phosphodiesterases as potential drug targets for anti-*Leishmania* therapy

RUNNING TITLE: PDEs: therapeutic targets for leishmaniasis

Victor Sebastián-Pérez,[a] Sarah Hendrickx,[b] Jane C. Munday,[c] Titilola Kalejaiye,[c] Ana Martínez,[a] Nuria E. Campillo,[a] Harry de Koning,[c] Guy Caljon,[b] Louis Maes[b,*] and Carmen Gil[a,*]

[a] Centro de Investigaciones Biológicas (CIB, CSIC). Ramiro de Maeztu, 9, 28040-Madrid, Spain

[b] Laboratory for Microbiology, Parasitology and Hygiene (LMPH), University of Antwerp, Belgium

[c] Institute of Infection, Inflammation and Immunity, College of Medical, Veterinary and Life Sciences, University of Glasgow, Glasgow, UK

Address correspondence to Carmen Gil, carmen.gil@csic.es, or Louis Maes, louis.maes@uantwerpen.be

ABSTRACT. The available treatments for leishmaniasis are less than optimal due to inadequate efficacy, toxic side-effects and the emergence of resistant strains, clearly endorsing the urgent need for discovery and development of novel drug candidates. Ideally, these should act via an alternative mechanism-of-action to avoid cross-resistance with the current drugs. As cyclic nucleotide specific phosphodiesterases (PDEs) of *L. major* have been postulated as putative drug targets, a series of potential inhibitors of *Leishmania* PDEs was explored. Several displayed potent and selective *in vitro* activity against *L. infantum* intracellular amastigotes. One imidazole derivative, compound **35**, was shown to reduce the parasite loads *in vivo* and dose-dependently increase the cellular cAMP level at just 2× and 5× the IC_{50}, indicating a correlation between antileishmanial activity and increased cellular cAMP. Docking studies and molecular dynamics simulations pointed to imidazole **35** exerting its activity through PDE inhibition. This study establishes for the first time that inhibition of cAMP PDEs can potentially be exploited for new antileishmanial chemotherapy.

KEYWORDS: Drug Discovery, Leishmaniasis, cAMP, PDEs

INTRODUCTION

Leishmaniasis is a group of diseases caused by trypanosomatid protozoans that belong to the genus *Leishmania*, of which more than 20 species are responsible for this poverty-associated disease. The clinical outcome can be grouped in two main forms: visceral leishmaniasis (VL) caused by *L. donovani* and *L. infantum*, and cutaneous leishmaniasis (CL) caused by *L. major*, *L. tropica* and *L. mexicana*, among other species. VL is fatal if left untreated, affecting vital organs such as liver, spleen and bone marrow. In contrast, CL causes the formation of ulcers that may heal spontaneously but leave permanent, disfiguring scars (1, 2). Leishmaniasis is a major health problem in tropical and subtropical countries where the sand fly vector is abundantly present. Although the disease has its main impact in developing countries of Southeast Asia, East Africa and Latin America, it is also endemic around the Mediterranean Sea (3). The rapid increase in cases of co-infection with HIV, facilitated by the impact of *Leishmania* on the immune system, is an increasing concern (4).

Despite ongoing efforts towards antileishmanial immunotherapy, a promising human vaccine has not yet been developed (5). This fact, together with the challenges in controlling the sandfly vectors (6), ensures that management of this neglected disease continues to rely almost exclusively on chemotherapy. Current treatments include pentavalent antimonials, liposomal amphotericin B, pentamidine, paromomycin and miltefosine. However, these drugs all have severe drawbacks relating to toxicity, stability, cost, and/or the spread of drug-resistant strains. With the exception of miltefosine, all require parenteral administration (7). Alternatives to the current drugs are therefore urgently needed. Ideally, drugs with a novel mechanism-of-action, able to overcome resistance to the current drugs, and oral administration are desirable (8-10).

Inhibitors of parasite enzymes that are homologous to human enzymes with a well-studied pharmacology may be a good starting point to look for new drugs, as such target-repurposing immediately unlocks a toolbox of potential inhibitors, enzyme structure assays and assorted other pharmacological and pharmaceutical know-how. With this in

mind, human phosphodiesterases (PDEs) are well studied enzymes essential for cyclic nucleotide signaling, whose druggability has been exploited in various human pathologies leading to several marketed drugs (11). Specific targeting of parasite PDEs could provide interesting options for the development of PDE inhibitors as antiprotozoal drugs (12, 13). PDEs are responsible for the hydrolysis of cyclic nucleotides, but their signaling role in trypanosomatids is not yet fully understood (14, 15). Since cyclic adenosine monophosphate (cAMP) is clearly involved in the pathogenesis (16), agents able to increase cAMP levels in the parasite, such as PDE inhibitors, may have therapeutic potential (17). Indeed, inhibition of PDEs was shown to lead to runaway cellular cAMP levels and cell death in several protozoan parasites (18-20), but this has yet not been investigated in *Leishmania*.

The *L. major* genome encodes five class-I PDEs: LmjPDEA, LmjPDEB1, LmjPDEB2, LmjPDEC and LmjPDED (21). LmjPDEA, LmjPDEB1 and LmjPDEB2 were shown to complement a cAMP-PDE-deficient yeast strain with LmjPDEB1 and LmjPDEB2 being cAMP-specific with the activity of LmjPDEA being lower and not fully characterized (22), although its overexpression in *L. donovani* decreased promastigote infectivity to macrophages and impacted on resistance to oxidative stress (23). The commercial PDE inhibitors dipyridamole, trequinsin and etazolate, were shown to inhibit LmjPDEB1 and LmjPDEB2, and the proliferation of *L. major* promastigotes *in vitro*; however, due to the high inhibitor concentrations needed for these effects, and the omission of a direct demonstration of any perturbation of the cellular cAMP concentration (22), ultimate validation of *Leishmania* PDEs as drug targets is still lacking.

Meanwhile, the X-ray structure of LmjPDEB1 showed a high level of similarity with the catalytic site of human PDEs but also revealed a parasite-specific sub-pocket (p-pocket) near the active site, which could afford the design of parasite-selective inhibitors (24). In the human PDEs this area is not accessible to inhibitors due to a lower volume and changes in the entry residues, which isolate it from the catalytic site. For this reason, this p-pocket would be very useful for the design of selective inhibitors. In *L.*

major PDEB1 this domain is formed by residues Met874 to Gly886, which act as its gating residues.

The present study presents selected human PDE inhibitors as pharmacological tools to validate the *Leishmania* PDEs as potential drug targets.

RESULTS

In vitro activity. A small focused library with 30 chemically diverse human cAMP PDE inhibitors, specifically inhibitors of PDE7A and PDE10A designed and synthesized in our laboratory, was evaluated phenotypically against a panel of three pathogenic trypanosomatids: *T. brucei*, *T. cruzi* and *L. infantum*. Cytotoxicity evaluation was carried out on human lung fibroblasts (MRC-5) and primary peritoneal mouse macrophages (PMM). A first selection included heterocyclic compounds with MW <500 Da and different scaffolds, such as quinazolines (Table 1) (25), furans (Table 2) (26), iminothiadiazoles (Table 3) (27), sulfides (Table 4) (28) and imidazoles (Table 5) (29). Only the imidazole compounds showed some inhibitory potential, and to check whether this core could be regarded as a privileged scaffold, 62 imidazole-related compounds from our MBC library (30) were evaluated next (Table 6). Four hits (**35**, **45**, **66** and **78**) were non-toxic to MRC-5 (CC_{50} >64 µM) with potent activity against intracellular amastigotes of *L. infantum* and/or *T. cruzi* (Fig. 1). Compounds **66** and **78** showed an IC_{50} in the same range as benznidazole (IC_{50} = 3.18 µM (31) against *T. cruzi*, while **45** and **35** confirmed against *L. infantum* with IC_{50} values below that of miltefosine (IC_{50} = 7.56 µM) (31).

[Here, tables 1-6, figure 1]

In vitro metabolic stability. The selected imidazoles were exposed to mouse S9 microsomal fractions to investigate the *in vitro* metabolic stability through Phase-I metabolism and Phase-II metabolism (Table 7). The *T. cruzi* hits **66** and **78** are both extensively metabolized through Phase-I metabolism with respectively 5% and 24% of

parent drug remaining after 15 min. Phase-II metabolism was less with 82% and 66% remaining after 15 min and about 50% after 60 min. For the *L. infantum* hits **45** and **35**, no extensive Phase-I nor Phase-II metabolism could be demonstrated, indicating satisfactory metabolic stability and suitability for *in vivo* follow-up evaluation. The reference drug diclofenac showed extensive Phase-I and -II metabolism, confirming proper functioning of the assay.

[Here, table 7]

Computational studies. To study the binding mode of imidazoles **35** and **45** in the LmjPDEB1 catalytic site, docking studies were performed as a starting point for dynamic simulations and were centered on a key residue of the catalytic site, Gln887. For both compounds, the best conformation binds the catalytic site of the enzyme, making key interactions with residues Gln887, Phe857 and Phe890 that allow the formation of a stable protein-ligand complex. In both complexes, the compounds appear to be able to target the parasite-specific pocket, as the docking studies show the methoxyphenyl substituent of either compound entering the p-pocket (Fig. 2). The best-ranked conformation of **35** was selected as starting point for the molecular dynamics studies. The results revealed stability of the complex, and to analyze the binding mode in detail, the interactions were monitored during the simulation time of 20ns. Most of the key interactions found in the docking pose were maintained throughout the run time, confirming that the hydrogen bond with Gln887 and the aromatic interactions with Phe857 and Phe890 provide the stability of the complex. Through this simulation process, it was also possible to identify some interactions with hydrophobic residues from the hydrophobic clamp. Importantly, the methoxy group was able to make a hydrogen bond with a residue inside the p-pocket, Asn881, as early as nanosecond 5 of the simulation, and this interaction was stably maintained during the rest of the simulation process (Fig. S1).

[Here, figure 2]

Efficacy in the *L. infantum* BALB/c mouse model. On the basis of the metabolic stability data and their possible interaction with *Leishmania* PDEB1, derivatives **35** and **45** were selected for a proof-of-concept *in vivo* assessment. Both were administered orally in the *L. infantum* Balb/c mouse model at 50 mg/kg b.i.d. for 5 days. Amastigote burdens in the target organs liver and spleen were determined on day 16-17 of the experiment (Table 8). The results are expressed as Leishman Donovan Units (LDU= mean number of amastigotes per liver/spleen cell per milligram of liver/spleen). The vehicle-treated controls showed high amastigote burdens in the liver (LDU = 618 ± 30) and lower burdens in the spleen (LDU = 16 ± 3) since the infection is primarily established in the liver around day 14 post-infection. Oral miltefosine (40 mg/kg s.i.d. for 5 days) displayed excellent activity, with parasite burdens in liver and spleen were reduced by 98.9% and 96.1%. Upon oral dosing at 50 mg/kg b.i.d. for 5 days, parasite burdens in liver and spleen were reduced by 32.4% and 38.9% for **45** and by 36.4% and 57.0% for **35**.

[Here, table 8]

In vitro cAMP measurements in *Leishmania* promastigotes. To establish whether imidazole **35** induces an intracellular cAMP increase in *L. infantum* promastigotes, the cAMP response was tested at a concentration corresponding to 2× and 5× its IC_{50} value against intracellular amastigotes. The experiment was performed on promastigotes since it is not possible to measure cAMP from intracellular amastigotes, with their cAMP content masked by that of the host cells, nor is it possible to obtain sufficient numbers of amastigotes from the infected animals without some host cell contamination. The chosen concentrations had no effect on promastigote viability over the 3 hours of the experiment. The compound induced a significant and dose-dependent increase in cellular cAMP

levels in the promastigotes (Fig. 3), consistent with inhibition of one or more PDEs in the same concentration range as its anti-leishmanial effects. The tetrahydrophthalazinone NPD0001, a potent inhibitor of *T. brucei* PDEB1 and TbrPDEB2 (18, 32) was used as positive control for a strong cAMP response.

[Here, figure 3]

DISCUSSION

One major health problem in tropical and subtropical countries is leishmaniasis, which is also endemic in the Mediterranean area. Although effective drugs exist for therapy, the side effects and the spread of drug-resistant strains make the discovery of novel drugs with a new mechanism-of-action urgent. It is increasingly argued that the search of new leishmanicidal agents should be based on well-known targets with established pharmacology, as such target repurposing greatly speeds up the drug discovery process; the cAMP PDEs fall into that category. The similarity between the human and protozoan enzymes, together with the availability of human PDEs inhibitors as reputable therapeutics, paved the way for the development of specific inhibitors of protozoan PDEs as potential drugs (33).

Based on this reasoning, and the powerful results obtained by the repurposing of human drugs for antitrypanosomatid therapy (34), thirty known inhibitors of human PDEs from our in-house library were initially selected and tested in a primary *in vitro* screening against a broad panel of pathogens and mammalian cell lines (Tables 1-5). Within our experience in the design and development of specific cAMP – hPDE inhibitors, this study specifically aimed at the identification of novel scaffolds for inhibition of protozoan PDEs. The finding that imidazoles with multiple phenyl substitutions showed a tendency to inhibit trypanosomatid growth triggered a subsequent screen of a larger focused library composed of 62 structurally related imidazoles (Table 6) and produced four hits (**35**, **45**, **66** and **78**). These compounds showed promising *in vitro* activity against *L. infantum* or

204 *T. cruzi* intracellular amastigotes with adequate selectivity with respect to cytotoxicity in
205 MRC-5 cells (SI = >12) (Fig. 1).
206 Metabolic stability of compounds in early drug development is one of the drug-
207 like properties used in candidate prioritization for progression (35) and directly supports
208 the *in vivo* follow-up experiments. To evaluate their suitability for *in vivo* evaluation, the
209 *in vitro* metabolic stability of the hit compounds was assessed using mouse S9
210 microsomal fraction, finding acceptable stability for both **35** and **45** (Table 7).
211 To investigate whether the selected compounds are able to bind the PDE catalytic site,
212 molecular modeling approaches were employed using the published LmjPDEB1 crystal
213 structure (2RQ8) (24). It is important to note that the *L. major* and *L. infantum* PDEB1s
214 are almost identical, displaying an identity of 95.7% between the full length open reading
215 frames and 97.4% for the catalytic domains (Fig. S2).
216 Docking calculations followed by molecular dynamics simulations evidenced that
217 these imidazole compounds are able to bind the active site of *Leishmania major* PDEB1.
218 In addition to interactions with the expected conserved residues, such as the hydrogen
219 bond with Gln887 and the aromatic interactions with Phe857 and Phe890, both
220 compounds were able to target the parasite-specific pocket through a bond between
221 their methoxyphenyl substituent and residue Asn881. This interaction with the p-pocket
222 is crucial for specificity over human PDEs and was maintained during a molecular
223 dynamics simulation (Fig. 2), opening new avenues for the specific design of PDE
224 parasitic inhibitors. To ascertain that the effect of the compounds was indeed the result
225 of PDE inhibition in the parasite, a measurable increase in cellular cAMP levels should
226 occur. Consistent with this expectation, imidazole **35** induced a significant dose-
227 dependent increase in the intracellular cAMP content of *L. infantum* promastigotes at
228 concentrations just above the antileishmanial IC_{50}, reaching a similar level as the potent
229 reference inhibitor NPD0001 (Fig. 4).
230 Metabolically stable imidazoles were advanced to the *L. infantum*-infected mouse
231 model. Oral treatment of 50 mg/kg b.i.d. for 5 days with compounds **35** or **45** displayed

a 30-60% reduction in the parasite burden, which represents only a moderate *in vivo* activity compared to miltefosine (Table 8). Yet, these encouraging results encourage further efforts towards optimization of the hit compounds by structure-aided medicinal chemistry, in order to improve drug-like properties such as oral bioavailability.

In conclusion, this is the first time that a PDE inhibitor with confirmed correlation between *in vitro* antileishmanial activity and cAMP content was shown to exhibit *in vivo* activity, which constitutes an important step towards establishing *Leishmania* PDEs as drug targets. Based on these results, imidazole derivatives can be regarded as promising hits to be developed in a hit-to-lead program to obtain new drug candidates for leishmaniasis with a better and safer pharmaceutical profile.

MATERIAL AND METHODS

Ethics statement: The use of laboratory rodents was carried out in strict accordance to all mandatory guidelines (EU directives, including the Revised Directive 2010/63/EU on the Protection of Animals used for Scientific Purposes that came into force on 01/01/2013, and the declaration of Helsinki in its latest version) and was approved by the ethical committee of the University of Antwerp, Belgium (UA-ECD 2016–54 (02/09/2016)).

Compounds studied: All the compounds tested in this work have a purity ≥95% by HPLC and are collected in the MBC chemical library (30). They were prepared in the Centro de Investigaciones Biológicas (CIB-CSIC) following previously described procedures: quinazolines (**1**-**7**) (25), furans (**8**-**12**) (26), iminothiadiazoles (**13**-**16**) (36), sulfides (**17**-**23**) (28) and imidazoles (**24**-**92**) (29).

In vitro parasite growth inhibition assays: An integrated screening was used to define the activity profile of the test compounds (**1**-**92**) adopting standard assay protocols as previously described (37). A brief description of each model is given. 1/ *Leishmania:* amastigotes harvested from the spleen of infected donor hamsters were used for infection. Murine peritoneal macrophages were obtained after intraperitoneal stimulation

with 2% starch in water for 24–48 h and plated in 96-well microplates at 10^4 cells/well. After adding 10^5 amastigotes per well and 5 days of incubation, parasite burdens are microscopically assessed after Giemsa staining*; 2/ African trypanosomes:* bloodstream forms of a drug sensitive *T. brucei* strain are axenically grown in Hirumi-9 medium at 37ºC under an atmosphere of 5% CO_2. Assays are performed in 96-well tissue culture plates, each well containing 10^4 parasites. After 4 days incubation, parasite growth is assessed by adding resazurin and fluorimetric reading after 4 h at 37ºC; 3/ *Chagas disease:* the nifurtimox-sensitive Tulahuen strain (Lac Z transfected) of *T. cruzi* is maintained on MRC-5 cells. Assays are performed in 96-well tissue culture plates, each well containing the compound dilutions together with 3×10^3 MRC-5 cells and 3×10^4 trypomastigotes. After 7 days incubation, colorimetric reading is performed after addition of chlorophenol red beta-D-galactopyranoside as substrate; 4/ Cytotoxicity: MRC-5 cells are cultured in MEM medium supplemented with 20 mM L-glutamine, 16.5 mM $NaHCO_3$ and 5% fetal calf serum. Assays are performed at 37ºC and 5% CO_2 in 96-well tissue culture plates with confluent monolayers. After 7 days incubation, cell proliferation and viability are assessed after addition of resazurin and fluorescence reading.

Microsomal stability assays: mouse liver microsomes (S9), NADPH generating system solutions and UGT reaction mix (BD Biosciences) were kept at -80°C. The test compounds (**35**, **45**, **66** and **78**), the internal standard tolbutamide and reference compound diclofenac were formulated in DMSO at 10 mM. The assay was carried out based on the BD Biosciences Guidelines for Use (TF000017 Rev1.0) with minor adaptations. The metabolic stability of the compounds was studied through the CYP_{450} superfamily (Phase-I metabolism) by fortification with reduced nicotinamide adenine dinucleotide phosphate (NADPH) and through uridine glucuronosyl transferase (UGT) enzymes (Phase-II metabolism) by fortification with uridine diphosphate glucuronic acid (UDPGA). For CYP_{450} and other NADPH dependent enzymes, the compounds were incubated at 5 µM together with 0.5 mg/mL S9 in potassium phosphate buffer in a reaction started by the addition of 1 mM NADP. At

288 defined time points, 20 µl was withdrawn from the reaction mixture and 80 µl cold
289 acetonitrile (ACN) was added to inactivate the enzymes and precipitate the protein.
290 The mixture was vortexed for 30 sec and centrifuged at 4ºC for 5 min to collect the
291 supernatant. For UGT enzymes, the compounds were incubated at 5 µM together
292 with 0.5 mg/mL S9 in a reaction started by the addition of 2mM UDPGA cofactor.
293 The loss of parent compound was determined using liquid chromatography (UPLC)
294 (Waters Aquity™) coupled with tandem quadrupole mass spectrometry (MS^2)
295 (Waters Xevo™), equipped with an electrospray ionization (ESI) interface and
296 operated in multiple reaction monitoring (MRM) mode.
297 Docking studies: Compounds **35** and **45** were prepared and converted into 3D for
298 computational studies using Ligprep tool (38), a module of Schrödinger software
299 package. All possible states at target pH 7.0 ± 1 were generated and stereoisomers and
300 low energy ring conformations were allowed during the process. The crystal structure
301 2R8Q (24) of LmjPDEB1 was retrieved from the Protein Data Bank and prepared using
302 the Protein Preparation Wizard tool (39) implemented on Maestro (40). Automated
303 docking was used to assess the appropriate binding orientations and conformations of
304 the ligand. A Lamarckian genetic algorithm (41) method implemented in the program
305 AutoDock 4.2 (42) was employed. For docking calculations, Gasteiger charges were
306 added, rotable bonds were set by AutoDock tools (ADT) and all torsions were allowed to
307 rotate for the ligand. In all the cases, we used grid maps with a grid box size of 60x60x60
308 $Å^3$ points and a grid-point spacing of 0.375 Å, using as centroid of the grid Gln887. The
309 docking protocol consisted of 100 independent Genetic Algorithm (GA) runs, population
310 size of 150, maximum number of evaluation 250000, while the other parameters were
311 default. Final best docked clusters, within the default 2.0 Å RMSD, according to the
312 binding energies and relative population provided by Autodock, were analyzed by visual
313 inspection. In both complexes, two main clusters were found in terms of energy, which
314 are also the most populated ones and therefore selected for further analysis (Figures S3
315 and S4).

316 Molecular Dynamics (MD) studies**:** Optimized Potentials for Liquid Simulations-2005
317 (OPLS2005) (43) force field in Desmond Molecular Dynamics System (44) was used as
318 force field to study the behavior of the ligand-target complex. The protein–ligand
319 complexes obtained from AutoDock docking protocol were prepared using Desmond set-
320 up wizard. For ligand **35**, QMESP charges were calculated using Jaguar software (45),
321 carrying out a geometry optimization with the basis set CC-PVTZ++. Charges were
322 added to the best docking output pose for further use. The system was solvated in a
323 triclinical periodic box of SPC water and then neutralized using an appropriate number
324 of counter ions. Also, a physiological NaCl concentration of 0.15M was added in the
325 system builder. The method selected for MD was NPT (Noose-Hover chain thermostat
326 at 300 K, Martyna-Tobias-Klein barostat at 1.01325 bar) no constrains were applied in
327 the MD protocol. Energy minimization of the prepared system was done up to a
328 maximum of 10 steps using steepest descent method or until a gradient threshold (25
329 kcal/mol/Å) was reached. Default protocol of Desmond was used to equilibrate the
330 system. Further MD simulations were carried out on these equilibrated systems for a
331 time period of 20 ns. The quality of MD simulations was assessed by the Simulation
332 Quality Analysis tools and analyzed by the Simulation Event Analysis tool, ligand–
333 receptor interactions were identified using the Simulation Interaction Diagram tool.
334 Energy fluctuations, RMSD and root-mean-square fluctuations (RMSF) of the complexes
335 in each trajectory were analyzed with respect to simulation time. Visualization and
336 analysis of the dynamics trajectories were performed using both Visual Molecular
337 Dynamics (VMD) (46) and Desmond Maestro simulation analysis tools.
338 cAMP determination in *Leishmania* promastigotes:
339 Promastigote in 24-well plates were incubated with either 2x or 5x IC_{50} of compound **35**
340 for 3 hours, initiated by adding 15 µL of each compound, at 100x concentration in 100%
341 DMSO to 1.5 ml culture. A 1.5-mL control culture received 15 µL of solvent (100%
342 DMSO). After 3 hours, a sample containing 5 x 10^6 cells was taken from each well and
343 centrifuged at 4500 x *g* for 10 min at 4°C and the supernatant was carefully removed.

For quantification of the intracellular cAMP, the cell pellet was immediately re-suspended in 100 µl 0.1 M HCl (by repeatedly pipetting up-and-down) and incubated on ice for 20 minutes in order to obtain complete cell lysis. The suspensions was then centrifuged at 10300 x *g* in a microfuge for 10 minutes at 4 °C and the supernatant (lysate) transferred to a fresh microfuge tube that was stored at -20 °C. The experiment was performed three times independently and all samples were assayed in duplicate using a Direct Cyclic AMP Enzyme Immunoassay kit (Assay Designs) according to the manufacturer's instructions.

Efficacy potential in the *L. infantum* BALB/c mouse model: female BALB/c mice (BW approx. 20 g) were purchased from a commercial source (Janvier France) and kept in quarantine for at least 5 days before starting the experiment. Food for laboratory rodents and drinking water were available *ad libitum*. The mice were randomly allocated to experimental units of 6 animals/group based on live body weight (BW) at the start of the experiment (Day 0 = day of infection). Spleen-derived *L. infantum* were purified using two centrifugation steps and diluted to prepare an infection inoculum containing 2 x 10^7 amastigotes/100µl phosphate buffered saline (PBS). The infection inoculum was administered by slow intravenous injection in the tail vein. The test compounds (**35** and **45**) were formulated in PEG_{400} at 25 mg/mL, envisaging dosing of 50 µL/25g. Miltefosine was formulated in water at 10 mg/mL, envisaging dosing of 100 µL/25g. The 5-day oral treatment started at day 7 post-infection and involved 4 groups: G1: PEG_{400} vehicle b.i.d. ; G2: miltefosine at 40 mg/kg s.i.d. ; G3: Comp. **45** at 50 mg/kg b.i.d. and G4: Comp. **35** at 50 mg/kg b.i.d. (50µL/25g). All animals were weighed twice weekly to monitor the general health status (severity of infection, toxicity of medication). Amastigote burdens in the target organs liver and spleen were determined on day 16-17 of the experiment. Organs of individual animals were weighed; impression smears were Giemsa-stained for microscopic evaluation of the total amastigote burden (= mean number of amastigotes per cell X number of cells counted (minimum 500 nuclei). Percentage reduction compared to the burdens in the vehicle-treated infected control animals is used as a

measure for drug activity.

ACKNOWLEDGEMENTS

Funding from the EC 7th Framework Programme (FP7-HEALTH-2013-INNOVATION-1, PDE4NPD no. 602666), MINECO (Grant SAF2015-65740-R), RICET (RD16/0027/0010), FEDER funds and MECD (Grant FPU15/1465 to V. S.-P.) is acknowledged. The authors thank Pim-Bart Feijens, Margot Desmet, Mandy Vermont and An Matheeussen for running the *in vitro* and *in vivo Leishmania* experiments.

REFERENCES

1. Pace D. 2014. Leishmaniasis. J Infect 69 Suppl 1:S10-18.
2. Savoia D. 2015. Recent updates and perspectives on leishmaniasis. J Infect Dev Ctries 9:588-596.
3. Alvar J, Velez ID, Bern C, Herrero M, Desjeux P, Cano J, Jannin J, den Boer M, Team WHOLC. 2012. Leishmaniasis worldwide and global estimates of its incidence. PLoS One 7:e35671.
4. Alvar J, Aparicio P, Aseffa A, Den Boer M, Canavate C, Dedet JP, Gradoni L, Ter Horst R, Lopez-Velez R, Moreno J. 2008. The relationship between leishmaniasis and AIDS: the second 10 years. Clin Microbiol Rev 21:334-359.
5. Srivastava S, Shankar P, Mishra J, Singh S. 2016. Possibilities and challenges for developing a successful vaccine for leishmaniasis. Parasit Vectors 9:277.
6. Bates PA, Depaquit J, Galati EA, Kamhawi S, Maroli M, McDowell MA, Picado A, Ready PD, Salomon OD, Shaw JJ, Traub-Cseko YM, Warburg A. 2015. Recent advances in phlebotomine sand fly research related to leishmaniasis control. Parasit Vectors 8:131.
7. Zulfiqar B, Shelper TB, Avery VM. 2017. Leishmaniasis drug discovery: recent progress and challenges in assay development. Drug Discovery Today 22:1516-1531.
8. Nagle AS, Khare S, Kumar AB, Supek F, Buchynskyy A, Mathison CJ, Chennamaneni NK, Pendem N, Buckner FS, Gelb MH, Molteni V. 2014. Recent developments in drug discovery for leishmaniasis and human African trypanosomiasis. Chem Rev 114:11305-11347.
9. Skinner-Adams TS, Sumanadasa SD, Fisher GM, Davis RA, Doolan DL, Andrews KT. 2016. Defining the targets of antiparasitic compounds. Drug Discovery Today 21:725-739.
10. de Koning HP. 2017. Drug resistance in protozoan parasites. Emerging Topics in Life Sciences 1:627-632.

409 11. Maurice DH, Ke H, Ahmad F, Wang Y, Chung J, Manganiello VC. 2014.
410 Advances in targeting cyclic nucleotide phosphodiesterases. Nat Rev Drug
411 Discovery 13:290-314.
412 12. Seebeck T, Sterk GJ, Ke H. 2011. Phosphodiesterase inhibitors as a new
413 generation of antiprotozoan drugs: exploiting the benefit of enzymes that are
414 highly conserved between host and parasite. Future Med Chem 3:1289-1306.
415 13. Shakur Y, de Koning HP, Ke H, Kambayashi J, Seebeck T. 2011. Therapeutic
416 potential of phosphodiesterase inhibitors in parasitic diseases. Handb Exp
417 Pharmacol 204:487-510.
418 14. Tagoe DN, Kalejaiye TD, de Koning HP. 2015. The ever unfolding story of cAMP
419 signaling in trypanosomatids: vive la difference! Front Pharmacol 6:185.
420 15. Gould MK, Bachmaier S, Ali JA, Alsford S, Tagoe DN, Munday JC, Schnaufer
421 AC, Horn D, Boshart M, de Koning HP. 2013. Cyclic AMP effectors in African
422 trypanosomes revealed by genome-scale RNA interference library screening for
423 resistance to the phosphodiesterase inhibitor CpdA. Antimicrob Agents
424 Chemother 57:4882-4893.
425 16. Salmon D, Vanwalleghem G, Morias Y, Denoeud J, Krumbholz C, Lhomme F,
426 Bachmaier S, Kador M, Gossmann J, Dias FB, De Muylder G, Uzureau P, Magez
427 S, Moser M, De Baetselier P, Van Den Abbeele J, Beschin A, Boshart M, Pays
428 E. 2012. Adenylate cyclases of Trypanosoma brucei inhibit the innate immune
429 response of the host. Science 337:463-466.
430 17. Makin L, Gluenz E. 2015. cAMP signalling in trypanosomatids: role in
431 pathogenesis and as a drug target. Trends Parasitol 31:373-379.
432 18. de Koning HP, Gould MK, Sterk GJ, Tenor H, Kunz S, Luginbuehl E, Seebeck T.
433 2012. Pharmacological validation of Trypanosoma brucei phosphodiesterases as
434 novel drug targets. J Infect Dis 206:229-237.
435 19. King-Keller S, Li M, Smith A, Zheng S, Kaur G, Yang X, Wang B, Docampo R.
436 2010. Chemical validation of phosphodiesterase C as a chemotherapeutic target

437 in Trypanosoma cruzi, the etiological agent of Chagas' disease. Antimicrob
438 Agents Chemother 54:3738-3745.
439 20. Kunz S, Balmer V, Sterk GJ, Pollastri MP, Leurs R, Muller N, Hemphill A, Spycher
440 C. 2017. The single cyclic nucleotide-specific phosphodiesterase of the intestinal
441 parasite Giardia lamblia represents a potential drug target. PLoS Negl Trop Dis
442 11:e0005891.
443 21. Gould MK, de Koning HP. 2011. Cyclic-nucleotide signalling in protozoa. FEMS
444 Microbiol Rev 35:515-541.
445 22. Johner A, Kunz S, Linder M, Shakur Y, Seebeck T. 2006. Cyclic nucleotide
446 specific phosphodiesterases of Leishmania major. BMC Microbiol 6:25.
447 23. Bhattacharya A, Biswas A, Das PK. 2008. Role of intracellular cAMP in
448 differentiation-coupled induction of resistance against oxidative damage in
449 Leishmania donovani. Free Radic Biol Med 44:779-794.
450 24. Wang H, Yan Z, Geng J, Kunz S, Seebeck T, Ke H. 2007. Crystal structure of the
451 Leishmania major phosphodiesterase LmjPDEB1 and insight into the design of
452 the parasite-selective inhibitors. Mol Microbiol 66:1029-1038.
453 25. Castaño T, Wang H, Campillo NE, Ballester S, Gonzalez-Garcia C, Hernandez
454 J, Perez C, Cuenca J, Perez-Castillo A, Martinez A, Huertas O, Gelpi JL, Luque
455 FJ, Ke H, Gil C. 2009. Synthesis, structural analysis, and biological evaluation of
456 thioxoquinazoline derivatives as phosphodiesterase 7 inhibitors.
457 ChemMedChem 4:866-876.
458 26. Redondo M, Brea JM, Perez DI, Soteras I, Val C, Perez C, Morales-Garcia JA,
459 Alonso-Gil S, Paul-Fernandez N, Martin-Alvarez R, Cadavid I, Loza I, Perez-
460 Castillo A, Mengod G, Campillo NE, Martinez A, Gil C. 2012. Effect of
461 phosphodiesterase 7 (PDE7) inhibitors in experimental autoimmune
462 encephalomyelitis mice. Discovery of a new chemically diverse family of
463 compounds. J Med Chem 55:3274-3284.

464 27. Redondo M, Palomo V, Brea J, Perez DI, Martin-Alvarez R, Perez C, Paul-
465 Fernandez N, Conde S, Cadavid MI, Loza MI, Mengod G, Martinez A, Gil C,
466 Campillo NE. 2012. Identification in silico and experimental validation of novel
467 phosphodiesterase 7 inhibitors with efficacy in experimental autoimmune
468 encephalomyelitis mice. ACS Chem Neurosci 3:793-803.
469 28. Garcia AM, Brea J, Morales-Garcia JA, Perez DI, Gonzalez A, Alonso-Gil S,
470 Gracia-Rubio I, Ros-Simo C, Conde S, Cadavid MI, Loza MI, Perez-Castillo A,
471 Valverde O, Martinez A, Gil C. 2014. Modulation of cAMP-specific PDE without
472 emetogenic activity: new sulfide-like PDE7 inhibitors. J Med Chem 57:8590-
473 8607.
474 29. Garcia AM, Salado IG, Perez DI, Brea J, Morales-Garcia JA, Gonzalez-Garcia A,
475 Cadavid MI, Loza MI, Luque FJ, Perez-Castillo A, Martinez A, Gil C. 2017.
476 Pharmacological tools based on imidazole scaffold proved the utility of PDE10A
477 inhibitors for Parkinson's disease. Future Med Chem 9:731-748.
478 30. Sebastian-Pérez V, Roca C, Awale M, Reymond, J.-L., Martínez A, Gil C,
479 Campillo NE. 2017. The Medicinal and Biological Chemistry (MBC) Library: an
480 efficient source on new hits. J Chem Inf Mod 57:2143-2151.
481 31. Kaiser M, Maes L, Tadoori LP, Spangenberg T, Ioset JR. 2015. Repurposing of
482 the Open Access Malaria Box for kinetoplastid diseases identifies novel active
483 scaffolds against Trypanosomatids. J Biomol Screen 20:634-645.
484 32. Veerman J, van den Bergh T, Orrling KM, Jansen C, Cos P, Maes L, Chatelain
485 E, Ioset JR, Edink EE, Tenor H, Seebeck T, de Esch I, Leurs R, Sterk GJ. 2016.
486 Synthesis and evaluation of analogs of the phenylpyridazinone NPD-001 as
487 potent trypanosomal TbrPDEB1 phosphodiesterase inhibitors and in vitro
488 trypanocidals. Bioorg Med Chem 24:1573-1581.
489 33. Martinez A, Gil C. 2018. Medicinal chemistry strategies to discover new
490 leishmanicidal drugs, p 153-178. *In* Rivas L, Gil C (ed), Drug Discovery for
491 Leishmaniasis. Royal Society of Chemistry, Cambridge.

492 34. Amata E, Xi H, Colmenarejo G, Gonzalez-Diaz R, Cordon-Obras C, Berlanga M,
493 Manzano P, Erath J, Roncal NE, Lee PJ, Leed SE, Rodriguez A, Sciotti RJ,
494 Navarro M, Pollastri MP. 2016. Identification of "Preferred" human kinase
495 inhibitors for sleeping sickness lead discovery. Are some kinases better than
496 others for inhibitor repurposing? ACS Infect Dis 2:180-186.
497 35. Hughes JP, Rees S, Kalindjian SB, Philpott KL. 2011. Principles of early drug
498 discovery. Br J Pharmacol 162:1239-1249.
499 36. Palomo V, Perez DI, Perez C, Morales-Garcia JA, Soteras I, Alonso-Gil S,
500 Encinas A, Castro A, Campillo NE, Perez-Castillo A, Gil C, Martinez A. 2012. 5-
501 Imino-1,2,4-thiadiazoles: first small molecules as substrate competitive inhibitors
502 of glycogen synthase kinase 3. J Med Chem 55:1645-1661.
503 37. Cos P, Vlietinck AJ, Berghe DV, Maes L. 2006. Anti-infective potential of natural
504 products: how to develop a stronger in vitro 'proof-of-concept'. J Ethnopharmacol
505 106:290-302.
506 38. LigPrep 3.1; Schrödinger, LLC: New York, 2014.
507 39. Schrödinger Suite 2015-4 Protein Preparation Wizard; Schrödinger Release
508 2015-4; Epik, S., LLC, New York, NY, 2015; Impact, Schrödinger, LLC, New York,
509 NY, 2015; Prime, Schrödinger, LLC, New York, NY, 2015.
510 40. Maestro, S., Schrödinger Release 2015-4; LLC, New York, NY, 2015.
511 41. Morris GM, Goodsell DS, Halliday RS, Huey R, Hart WE, Belew RK, Olson AJ.
512 1998. Automated docking using a Lamarckian genetic algorithm and an empirical
513 binding free energy function. J Comput Chem 19:1639-1662.
514 42. Morris GM, Huey R, Lindstrom W, Sanner MF, Belew RK, Goodsell DS, Olson
515 AJ. 2009. AutoDock4 and AutoDockTools4: Automated docking with selective
516 receptor flexibility. J Comput Chem 30:2785-2791.
517 43. Banks JL, Beard HS, Cao Y, Cho AE, Damm W, Farid R, Felts AK, Halgren TA,
518 Mainz DT, Maple JR, Murphy R, Philipp DM, Repasky MP, Zhang LY, Berne BJ,

519 Friesner RA, Gallicchio E, Levy RM. 2005. Integrated Modeling Program, Applied
520 Chemical Theory (IMPACT). J Comput Chem 26:1752-1780.
521 44. Desmond Molecular Dynamics System, D. E. S. R., Schrödinger Release 2015-
522 4, New York, NY, 2015. Maestro-Desmond Interoperability Tools, Schrödinger,
523 New York, NY, 2015.
524 45. Jaguar, S., Schrödinger Release 2015-4; LLC, New York, NY, 2015.
525 46. Humphrey W, Dalke A, Schulten K. 1996. VMD: Visual molecular dynamics. J
526 Mol Graph 14:33-38.

527

Figure Legends

Figure 1. Selected imidazole hits for further studies.

Figure 2. Docking results for imidazoles **35** (cyan) and **45** (yellow) in LmjPDEB1: global view of the protein, zoom in the catalytic binding site, key residues and the p-pocket in a grey circle are shown.

Figure 3. Intracellular cAMP in *L. infantum* promastigotes after 3 h of incubation. Imidazole **35** was used at 2x and at 5x the IC_{50} concentration of 5.1 µM.

Table 1. *In vitro* antiparasitic activities (IC_{50}-values, µM) of quinazoline-like hPDE7A inhibitors.

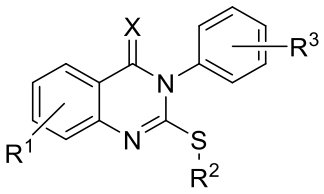

Comp.	X	R^1	R^2	R^3	IC_{50}(hPDE7A) (25)	MRC-5	*T. cruzi*	*L. inf*	*T. brucei*	PMM
1	S	H	H	H	0.6 µM	>64.0	51.5	>64.0	60.6	>64.0
2	S	H	Me	2-Br	5.3 µM	3.2	5.0	>64.0	33.4	-
3	O	6-Br	H	2,6-diF	11.0 µM	>64.0	>64.0	>64.0	>64.0	-
4	O	H	H	H	4.7 µM	>64.0	>64.0	>64.0	37.4	>64.0
5	O	H	Me	2,6-diF	4.7 µM	29.3	>64.0	>64.0	51.7	>64.0
6	O	8-Me	H	2-Br	2.0 µM	>64.0	>64.0	>64.0	>64.0	>64.0
7	O	6-Br	Me	2-Br	0.7 µM	6.7	8.6	26.4	19.4	32.0

IC_{50} values for inhibition of the growth of *T. cruzi*, *L. infantum*, and *T. brucei* or for cytotoxicity toward human lung fibroblasts (MRC-5 cells) and primary peritoneal mouse macrophages (PMM); Each value is the mean of two independent determinations

Table 2. *In vitro* antiparasitic activities (IC_{50}-values, µM) of furan-like hPDE7A inhibitors.

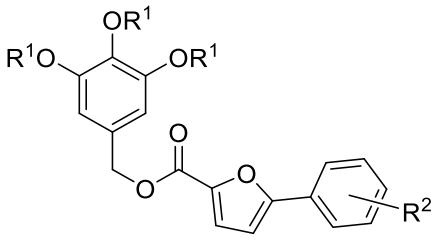

Comp.	R^1	R^2	IC_{50}(hPDE7A) (26)	MRC-5	*T. cruzi*	*L. inf*	*T. brucei*	PMM
8	Me	H	5.2 µM	>64.0	>64.0	>64.0	>64.0	>64.0
9	Me	4-Cl,2-NO_2	7.3 µM	35.5	33.0	>64.0	34.0	-
10	Me	2,4-diCl	38%@10 µM	>64.0	>64.0	>64.0	57.4	>64.0
11	Me	4-Me	30%@10 µM	28.6	>64.0	>64.0	62.9	>64.0
12	Et	H	30%@10 µM	>64.0	24.5	33.2	30.3	>64.0

IC_{50} values for inhibition of the growth of *T. cruzi*, *L. infantum*, and *T. brucei* or for cytotoxicity toward human lung fibroblasts (MRC-5 cells) and primary peritoneal mouse macrophages (PMM); Each value is the mean of two independent determinations.

Table 3. *In vitro* antiparasitic activities (IC_{50}-values, µM) of iminothiadiazole-like hPDE7A inhibitors.

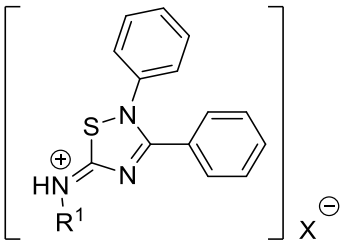

Comp.	R^1	X	IC_{50}(hPDE7A) (27)	MRC-5	*T. cruzi*	*L. inf*	*T. brucei*	PMM
13	-CH_2CH_2-OH	Br	1.1 µM	29.3	48.2	32.5	>64.0	32.0
14	-$(CH_2)_2$-Morph	2Br	1.6 µM	30.3	48.3	32.5	60.0	32.0
15	-CH_2-3Pyr	2Br	0.4 µM	7.5	8.1	26.4	35.7	32.0
16	H	Br	1.0 µM	30.1	32.3	32.5	39.2	32.0

IC_{50} values for inhibition of the growth of *T. cruzi*, *L. infantum*, and *T. brucei* or for cytotoxicity toward human lung fibroblasts (MRC-5 cells) and primary peritoneal mouse macrophages (PMM); Each value is the mean of two independent determinations.

Table 4. *In vitro* antiparasitic activities (IC_{50}-values, µM) of sulphide-like hPDE7A inhibitors.

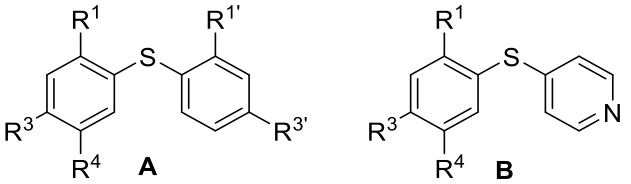

Comp.	form	R^1	R^3	R^4	$R^{1'}$	$R^{3'}$	IC_{50}(hPDE7A) (28)	MRC-5	*T. cruzi*	*L. Inf*	*T. brucei*	PMM
17	A	NO_2	Cl	H	H	NH_2	0.4 µM	>64.0	>64.0	>64.0	48.0	>64.0
18	B	NO_2	Cl	H	-	-	0.7 µM	>64.0	27.2	12.7	19.1	-
19	A	NO_2	Cl	H	Br	H	1.0 µM	>64.0	28.8	38.0	32.0	-
20	A	NO_2	H	Cl	NHAc	H	2.1 µM	>64.0	50.9	>64.0	>64.0	>64.0
21	A	Cl	NO_2	H	NH_2	H	8.8 µM	35.3	29.0	>64.0	32.6	>64.0
22	A	NO_2	H	Cl	Br	H	1.0 µM	16.9	22.9	51.0	32.9	>64.0
23	B	Cl	NO_2	H	-	-	0.2 µM	>64.0	36.7	>64.0	47.3	>64.0

IC_{50} values for inhibition of the growth of *T. cruzi*, *L. infantum*, and *T. brucei* or for cytotoxicity toward human lung fibroblasts (MRC-5 cells) and primary peritoneal mouse macrophages (PMM); Each value is the mean of two independent determinations

Table 5. *In vitro* antiparasitic activities (IC_{50}-values, µM) of imidazole-like hPDE10A inhibitors.

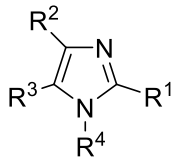

Comp.	R^1	R^2	R^3	R^4	IC_{50}(hPDE10A) (29)	MRC-5	*T. cruzi*	*L. inf*	*T. brucei*
24	3,4-diCF_3-Ph	4-OMe-Ph	H	H	0.4 µM	15.4	6.1	32.2	2.0
25	2-Cl-Ph	4-Br-Ph	4-Br-Ph	H	20 nM	>64.0	2.2	50.8	2.2
26	4-Cl-Ph	4-OMe-Ph	H	H	2.0 µM	19.8	17.8	26.4	29.6
27	H	4-Br-Ph	4-Br-Ph	H	0.2 µM	42.5	>64.0	32.5	>64.0
28	2-Br-Ph	4-Br-Ph	4-Br-Ph	H	0.4 µM	>64.0	18.0	>64.0	8.2
29	Ph	Ph	Ph	Me	4.1 µM	50.6	8.2	20.6	20.2
30	2-Br-Ph	4-OMe-Ph	4-OMe-Ph	H	2.2 µM	>64.0	7.3	14.3	7.5

IC_{50} values for inhibition of the growth of *T. cruzi*, *L. infantum*, and *T. brucei* or for cytotoxicity toward human lung fibroblasts (MRC-5 cells) and primary peritoneal mouse macrophages (PMM); Each value is the mean of two independent determinations

Table 6. *In vitro* antiparasitic activities (IC_{50}-values, µM) of imidazole derivatives from MBC library.

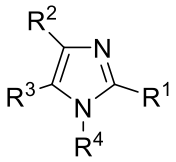

Comp.	R^1	R^2	R^3	R^4	MRC-5	*T. cruzi*	*L. inf*	*T.*
31	2-OMe-Ph	4-Br-Ph	4-Br-Ph	H	>64.0	>64.0	48.2	>
32	3-Cl-Ph	4-Br-Ph	4-Br-Ph	H	45.8	>64.0	7.5	2
33	4-Cl-Ph	4-Br-Ph	4-Br-Ph	H	>64.0	>64.0	20.3	>
34	Ph	4-Br-Ph	4-Br-Ph	H	>64.0	>64.0	48.2	>
35	2,4-diOMe-Ph	4-Br-Ph	4-Br-Ph	H	>64.0	7.6	5.2	1
36	2,5-diOMe-Ph	4-Br-Ph	4-Br-Ph	H	>64.0	17.8	15.0	1
37	2-OMe-Ph	4-Br-Ph	4-Br-Ph	Bn	>64.0	6.8	6.7	8
38	2-Cl-Ph	4-Br-Ph	4-Br-Ph	Bn	>64.0	14.2	9.4	8
39	2,4-diOMe-Ph	4-Br-Ph	4-Br-Ph	Me	36.4	51.3	18.8	8
40	2,5-diOMe-Ph	4-Br-Ph	4-Br-Ph	Et	>64.0	18.7	16.5	3
41	2-Cl-Ph	4-OMe-Ph	4-OMe-Ph	H	>64.0	7.9	16.5	7
42	2-OMe-Ph	4-OMe-Ph	4-OMe-Ph	H	>64.0	>64.0	48.2	>
43	Ph	4-OMe-Ph	4-OMe-Ph	H	6.3	8.1	5.9	6
44	2-OMe-Ph	4-OMe-Ph	4-OMe-Ph	Bn	>64.0	4.6	6.7	7
45	2-Cl-Ph	4-OMe-Ph	4-OMe-Ph	Bn	>64.0	5.1	5.1	8
46	Ph	Ph	Ph	H	52.5	>64.0	>64.0	>
47	Ph	Ph	Ph	Et	31.2	47.4	42.1	4
48	Ph	Ph	H	H	55.1	47.9	>64.0	>
49	2,4,5-triOMe-Ph	Ph	H	H	19.3	39.2	29.8	2
50	2,4-diOMe-Ph	Ph	H	H	16.6	49.4	35.2	3
51	2,5-diOMe-Ph	Ph	H	H	28.9	33.3	48.2	2
52	2-OMe-Ph	Ph	H	H	30.7	50.6	32.8	5
53	3-Me-Ph	Ph	H	H	30.4	29.5	20.3	2
54	4-F-Ph	Ph	H	H	21.9	48.3	32.5	2
55	4-Me-Ph	Ph	H	H	10.6	28.8	29.9	2
56	2-Cl-Ph	Ph	H	H	37.2	49.1	48.2	>
57	3-Me-Ph	Ph	H	Bn	>64.0	20.3	26.7	2
58	4-Me-Ph	Ph	H	Bn	49.3	7.0	20.4	8
59	2,4,5-triOMe-Ph	Ph	H	Bn	29.0	18.6	12.0	3
60	2-Cl-Ph	Ph	H	Bn	28.5	7.8	53.53	8
61	Ph	2-naphtyl	H	H	35.7	54.9	36.05	>
62	Ph	4-OMe-Ph	H	H	13.9	31.8	48.23	3
63	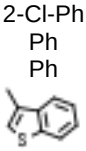	4-OMe-Ph	H	H	4.9	11.5	20.28	2
64		4-Br-Ph	H	H	7.2	7.9	20.28	8
65	Ph	4-Br-Ph	H	H	5.5	8.5	48.2	2
66	2-Pyr	4-Br-Ph	H	H	>64.0	4.7	14.6	1
67	3,5-diCF_3-Ph	4-Br-Ph	H	H	3.5	5.5	2.0	2
68	4-Cl-Ph	4-Cl-Ph	H	H	10.1	8.7	20.3	9
69	4-Cl-Ph	4-Cl-Ph	H	Bn	>64.0	9.1	20.3	9
70	Ph	4-Cl-Ph	H	Bn	61.6	7.7	16.51	8
71	3,5-diCF_3-Ph	3-Pyr	H	H	>64.0	>64.0	48.2	2
72	H	4-OMe-Ph	4-OMe-Ph	H	5.9	46.3	>64.0	>
73	H	Me	Ph	H	>64.0	>64.0	>64.0	>
74	H	Ph	Ph	H	>64.0	>64.0	>64.0	>
75	H	Ph	Ph	Me	>64.0	48.7	35.6	>
76	H	Ph	Ph	Et	25.8	46.5	32.5	>
77	H	Ph	Ph	Bu	32.3	22.9	23.7	3
78	H	Ph	Ph	CH_2-4-Cl-Ph	>64.0	4.5	48.0	8
79	H	Ph	Ph	CH_2-4-CF_3-Ph	>64.0	15.7	42.2	9

80	H	Ph	Ph	CH_2-2-Cl-Ph	14.1	18.2	>64.0	2
81	H	Ph	Ph	Bn	12.2	19.6	38.3	2
82	H	Ph	Ph	CH_2-biPh	6.7	7.9	36.0	2
83	H	Ph	Ph	CH_2-4-Pyr	44.4	47.4	48.2	3
84	H	Ph	Ph	CH_2-3-Cl-Ph	8.0	20.4	42.2	8
85	H	Ph	Ph	CH_2-4-SMe-Ph	>64.0	>64.0	>64.0	>
86	H	Ph	Ph	CO-Ph	>64.0	>64.0	48.2	>
87	H	Ph	Ph	CH_2-3,4-diCF_3-Ph	6.2	5.0	8.6	8
88	H	4-Br-Ph	H	H	>64.0	47.0	>64.0	>
89	H	4-Br-Ph	H	Bn	>64.0	47.8	49.3	3
90	H	4-Br-Ph	H	CH_2-3,4-diCF_3-Ph	>64.0	>64.0	>64.0	8
91	H	Ph	H	Bn	48.8	48.7	48.2	5
92	H	4-F-Ph	H	Bn	20.0	48.2	45.6	3

IC_{50} values for inhibition of the growth of *T. cruzi*, *L. infantum*, and *T. brucei* or for cytotoxicity toward human lung fibroblasts (MRC-5 cells) and primary peritoneal mouse macrophages (PMM); Each value is the mean of two independent determinations

Table 7. *In vitro* metabolic stability: percentage of parent compounds over time in the presence of mouse liver microsomes.

		% parent compound remaining upon incubation									
Phase I/II	Time (min)	Comp. **35**		Comp. **45**		Comp. **66**		Comp. **78**		**Diclofenac**	
		Average	Stdev	Average	Stdev	Average	Stdev	Average	Stdev	Average	Stdev
CYP_{450}-NADPH	0	100	-	100	-	100	-	100	-	100	-
	15	103	3.6	128	24.6	5	0.8	24	11.5	83	22.7
	30	100	0.5	109	25.8	2	0.2	4	2.8	68	20.5
	60	81	2.0	168	79.5	2	0.2	2	1.5	61	20.4
		(n=3)		(n=3)		(n=3)		(n=3)		(n=3)	
UGT enzymes	0	100	-	100	-	100	-	100	-	100	-
	15	102	9.4	90	9.2	82	3.0	66	20.8	35	5.9
	30	99	9.4	76	25.6	64	9.3	59	26.9	38	2.1
	60	104	10.8	62	19.3	53	9.9	50	28.7	51	27.8
		(n=3)		(n=3)		(n=3)		(n=3)		(n=3)	

Table 8. *In vivo* activity of the imidazoles **45** and **35** in the *L. infantum* BALB/c mouse model (organ burdens and percentage of efficacy).

Dosing group	Liver amastigote burden		Spleen amastigote burden	
	Mean ± SD LDU	%Reduction	Mean ± SD LDU	%Reduction
G1: Vehicle: PEG 400	618 ± 30	-	16 ± 3	-
G2: **Miltefosine** at 40 mg/Kg s.i.d. PO for 5 days	7 ± 2	**98.9**	1 ± 0	**96.1**
G3: Comp. **45** at 50 mg/Kg b.i.d. PO for 5 days	418 ± 56	**32.4**	10 ± 2	**38.9**
G4: Comp. **35** at 50 mg/Kg b.i.d. PO for 5 days	393 ± 28	**36.4**	7 ± 1	**57.0**

SUPPORTING INFORMATION

Cyclic nucleotide specific phosphodiesterases as potential drug targets for anti-*Leishmania* therapy

Victor Sebastián-Pérez,[a] Sarah Hendrickx,[b] Jane C. Munday,[c] Titilola Kalejaiye,[c] Ana Martínez,[a] Nuria E. Campillo,[a] Harry de Koning,[c] Guy Caljon,[b] Louis Maes[b,*] and Carmen Gil[a,*]

[a] Centro de Investigaciones Biológicas (CIB, CSIC). Ramiro de Maeztu, 9, 28040-Madrid, Spain

[b] Laboratory for Microbiology, Parasitology and Hygiene (LMPH), University of Antwerp, Belgium

[c] Institute of Infection, Inflammation and Immunity, College of Medical, Veterinary and Life Sciences, University of Glasgow, Glasgow, UK

Address correspondence to Carmen Gil, carmen.gil@csic.es, or Louis Maes, louis.maes@uantwerpen.be

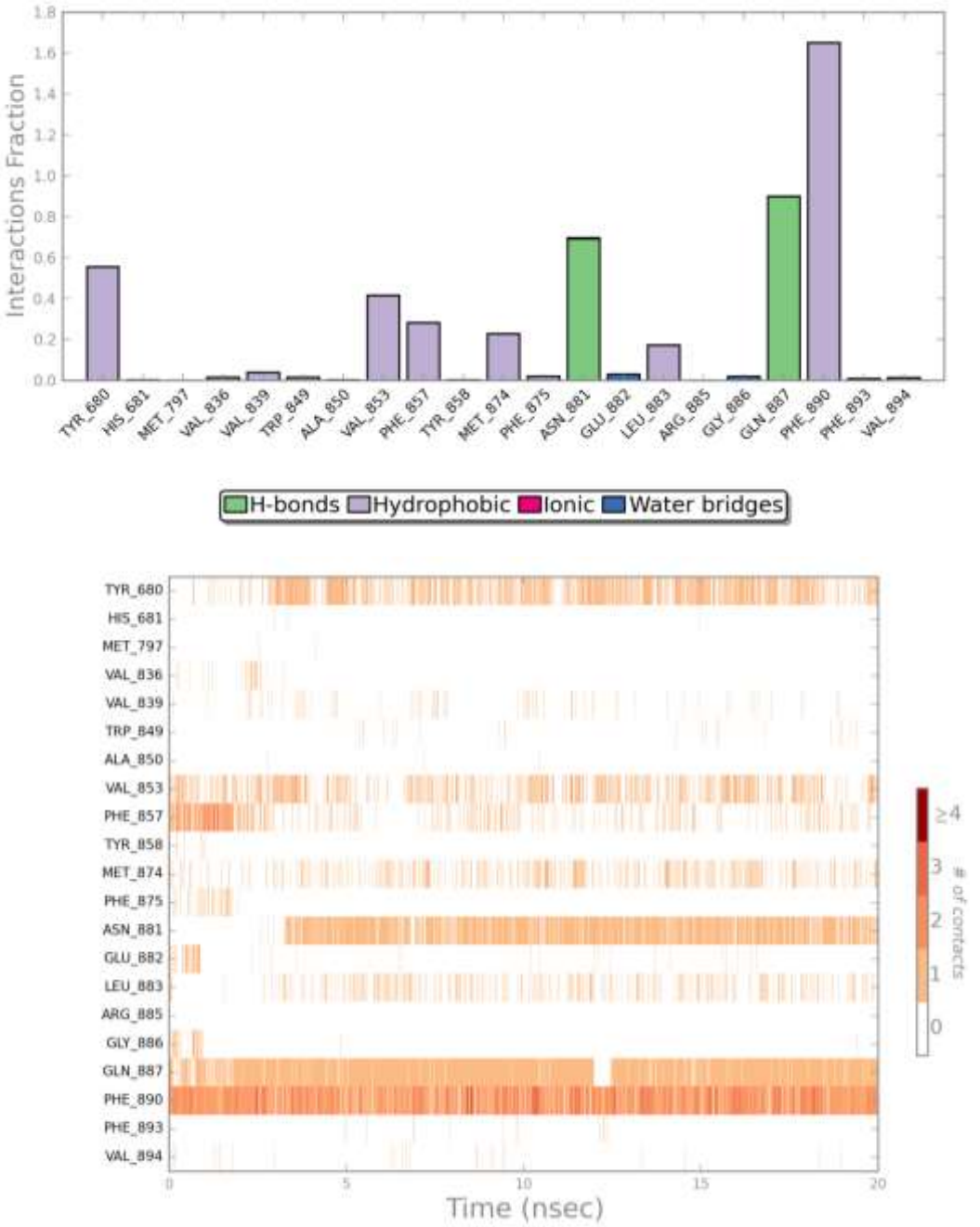

Figure S1. Interactions found during the simulation process. Key interactions present in the docking result are maintained during the simulation and a new interaction in the p-pocket is established.

```
CLUSTAL O(1.2.4) multiple sequence alignment FULL-LENGTH PROTEIN


tr|A4HWN7|A4HWN7_LEIIN      MYSAVFSPAAPYCGVAGSSHLCEAVALCQSILARYRRTGTSFSSTELKAIQALRTELPDT   60
tr|Q6S996|Q6S996_LEIMA      MHSAVFSPDAPYCGAAGSNHLCEAVALCQSILARYRRTGTSFSSTELKAIQALRTEFPDT   60
                            *:****** *****.***.************************************:***

tr|A4HWN7|A4HWN7_LEIIN      AQGPAANSAGSPHQTTNDLLNILDDATDMPHNPHDDIVAFVEECCDNTKDPTVLFAAINE   120
tr|Q6S996|Q6S996_LEIMA      AQEPAANSAASPDQTTKDFLSILDDATDVPHNPQNDIVAFVEECCDNTKEPTVLFAAINE   120
                            ** ******.**.***:*:*.*******:****::**************:**********

tr|A4HWN7|A4HWN7_LEIIN      RISAVTCSRNVRTYMVITNDNLLWDPVNGVAALIDDVTPLGKCAQAHNMLTIASTLYIPL   180
tr|Q6S996|Q6S996_LEIMA      RISAVTCSRNVRTYMVIANDNLLWDPVNGVAALIDDVTPLGKCAQARNMLTIANTLYIPL   180
                            *****************:*****************************:******.******

tr|A4HWN7|A4HWN7_LEIIN      WFRSELVGCVEAPSGCIPRDKATYAQLLLRSVTVAVRNSINISIRKSEANKIEAMVSMAT   240
tr|Q6S996|Q6S996_LEIMA      WFRSELVGCVEVPGACIPRDKATCAQLLLRCVTVAVRNSINISIRKREANKIEAMVGMAT   240
                            ***********.*..******** ******.*************** *********.***

tr|A4HWN7|A4HWN7_LEIIN      RLARDTLEESVLVQSIINTAKKLTESDRCSIFLVKADGSLEAHFEDGNVVVLPAGTGIAG   300
tr|Q6S996|Q6S996_LEIMA      RLARDTLEESVLVQSIINTAKTLTESDRCSIFLVKADGSLEAHFEDGNVVVLPAGTGIAG   300
                            **********************.****************************************

tr|A4HWN7|A4HWN7_LEIIN      HVVESGAVVNIPNAYEDERFNRSVDKVTGYHTRTILCLPIAFEGTIVAVAQLINKLDMVT   360
tr|Q6S996|Q6S996_LEIMA      HVAESGAVVNIPNAYEDDRFHRSVDKVTGYHTRTILCLPIAFEGTIVAVAQLINKLDMVT   360
                            **.**************:**:****************************************

tr|A4HWN7|A4HWN7_LEIIN      QSGQRLPRVFGRRDEELFETFSMFAAASLRNCRINETLLKEKKKSDAILDVVALLSNTDI   420
tr|Q6S996|Q6S996_LEIMA      QSGQRLPRVFGRRDEELFETFSMFAAASLRNCRINETLLKEKKKSDAILDVVALLSNTDI   420
                            ************************************************************

tr|A4HWN7|A4HWN7_LEIIN      RDVDSIVRHVLHGAKKLLNADRSSMFLLDKERNELYSKMADSANEIRFPCGQGIAGTVAE   480
tr|Q6S996|Q6S996_LEIMA      RDVDSIVRHVLHGAKKLLNADRSSMFLLDKERNELYSKMADSANEIRFPCGQGIAGTVAE   480
                            ************************************************************

tr|A4HWN7|A4HWN7_LEIIN      SGVGENIMDAYADSRFNSAVDRQLGYRTQSILCEPIMLNGEVLAVVQLVNKLGDDGSVTC   540
```

```
tr|Q6S996|Q6S996_LEIMA      SGVGENIMDAYADSRFNSAVDRQLGYRTQSILCEPITLNGEVLAVVQLVNKLGDDGSVTC   540
                            ********************************** **********************

tr|A4HWN7|A4HWN7_LEIIN      FTPMDRETFQVFSLFAGISINNSHLLEFAVNAGREAMTLSLQRNSITAQRAPKRVKVIAV   600
tr|Q6S996|Q6S996_LEIMA      FTPMDRETFQVFSLFAGISINNSHLLEFAVNAGREAMTLSLQRNSITAQRAPKSVKVIAV   600
                            ************************************************** ******

tr|A4HWN7|A4HWN7_LEIIN      TPEEREAVMSIDFGDAYDFTSPDFNLFEVREKYSEPMDAAAGVVYNLLWSSGLPEKFGCR   660
tr|Q6S996|Q6S996_LEIMA      TPEEREAVMSIDFGGAYDFTSPGFNLFEVREKYSEPMDAAAGVVYNLLWNSGLPEKFGCR   660
                            **************.*******.*************************.**********

tr|A4HWN7|A4HWN7_LEIIN      EQTLLNFILQCRRRYRRVPYHNFYHVVDVCQTLHTYLYTGKASELLTELECYVLLVTALV   720
tr|Q6S996|Q6S996_LEIMA      EQTLLNFILQCRRRYRRVPYHNFYHVVDVCQTLHTYLYTGKASELLTELECYVLLVTALV   720
                            ************************************************************

tr|A4HWN7|A4HWN7_LEIIN      HDLDHMGVNNSFYLKTDSPLGILSSASGNNSVLEVHHCSLAIEILSDPAADVFEGLSGQD   780
tr|Q6S996|Q6S996_LEIMA      HDLDHMGVNNSFYLKTDSPLGILSSASGNNSVLEVHHCSLAIEILSDPAADVFEGLSGQD   780
                            ************************************************************

tr|A4HWN7|A4HWN7_LEIIN      VAYAYRALIDCVLATDMAKHADALSRFTELATSGFDKENEAHRRMVMETLIKAGDVSNVT   840
tr|Q6S996|Q6S996_LEIMA      VAYAYRALIDCVLATDMAKHADALSRFTELATSGFEKDNDTHRRLVMETLIKAGDVSNVT   840
                            ************************************:*:*::***:***************

tr|A4HWN7|A4HWN7_LEIIN      KPFETSRMWAMAVTEEFYRQGDMEKEKGVEVLPMFDRSKNNELARGQIGFIDFVAGKFFR   900
tr|Q6S996|Q6S996_LEIMA      KPFETSRMWAMAVTEEFYRQGDMEKEKGVEVLPMFDRSKNNELARGQIGFIDFVAGKFFR   900
                            ************************************************************

tr|A4HWN7|A4HWN7_LEIIN      DIVGNLFHGMQWCVDTVNSNRAKWQEILDGRRDSTRSSIV 940
tr|Q6S996|Q6S996_LEIMA      DIVGNLFHGMQWCVDTVNSNRAKWQEILDGRRDSIRSSIV 940
                            ********************************** *****
```

Percent Identity Matrix

1: tr|A4HWN7|A4HWN7_LEIIN	100.00	95.74
2: tr|Q6S996|Q6S996_LEIMA	95.74	100.00

```
CLUSTAL O(1.2.4) multiple sequence alignment CATALYTIC DOMAIN


tr|A4HWN7|A4HWN7_LEIIN      TPEEREAVMSIDFGDAYDFTSPDFNLFEVREKYSEPMDAAAGVVYNLLWSSGLPEKFGCR     60
tr|Q6S996|Q6S996_LEIMA      TPEEREAVMSIDFGGAYDFTSPGFNLFEVREKYSEPMDAAAGVVYNLLWNSGLPEKFGCR     60
                            **************.*******.*************************.**********

tr|A4HWN7|A4HWN7_LEIIN      EQTLLNFILQCRRRYRRVPYHNFYHVVDVCQTLHTYLYTGKASELLTELECYVLLVTALV     120
tr|Q6S996|Q6S996_LEIMA      EQTLLNFILQCRRRYRRVPYHNFYHVVDVCQTLHTYLYTGKASELLTELECYVLLVTALV     120
                            ************************************************************

tr|A4HWN7|A4HWN7_LEIIN      HDLDHMGVNNSFYLKTDSPLGILSSASGNNSVLEVHHCSLAIEILSDPAADVFEGLSGQD     180
tr|Q6S996|Q6S996_LEIMA      HDLDHMGVNNSFYLKTDSPLGILSSASGNNSVLEVHHCSLAIEILSDPAADVFEGLSGQD     180
                            ************************************************************

tr|A4HWN7|A4HWN7_LEIIN      VAYAYRALIDCVLATDMAKHADALSRFTELATSGFDKENEAHRRMVMETLIKAGDVSNVT     240
tr|Q6S996|Q6S996_LEIMA      VAYAYRALIDCVLATDMAKHADALSRFTELATSGFEKDNDTHRRLVMETLIKAGDVSNVT     240
                            ************************************:*:*::***:***************

tr|A4HWN7|A4HWN7_LEIIN      KPFETSRMWAMAVTEEFYRQGDMEKEKGVEVLPMFDRSKNNELARGQIGFIDFVAGKFFR     300
tr|Q6S996|Q6S996_LEIMA      KPFETSRMWAMAVTEEFYRQGDMEKEKGVEVLPMFDRSKNNELARGQIGFIDFVAGKFFR     300
                            ************************************************************

tr|A4HWN7|A4HWN7_LEIIN      DIVGNLFHGMQWCVDTVNSNRAKWQEILDGRRDSTRSSIV        340
tr|Q6S996|Q6S996_LEIMA      DIVGNLFHGMQWCVDTVNSNRAKWQEILDGRRDSIRSSIV        340
                            ********************************* *****


  Percent Identity  Matrix

     1: tr|A4HWN7|A4HWN7_LEIIN  100.00   97.35
     2: tr|Q6S996|Q6S996_LEIMA   97.35  100.00
```

Figure S2. Phosphodiesterase sequences alignment in *Leishmania infantum* (Uniprot code: A4HWN7) and *Leishmania major* (Uniprot code: Q6S996). Full length sequence and catalytic domain are aligned respectively. Identity matrices regarding sequence identity between both proteins, in the full length and the catalytic domain, are also shown.

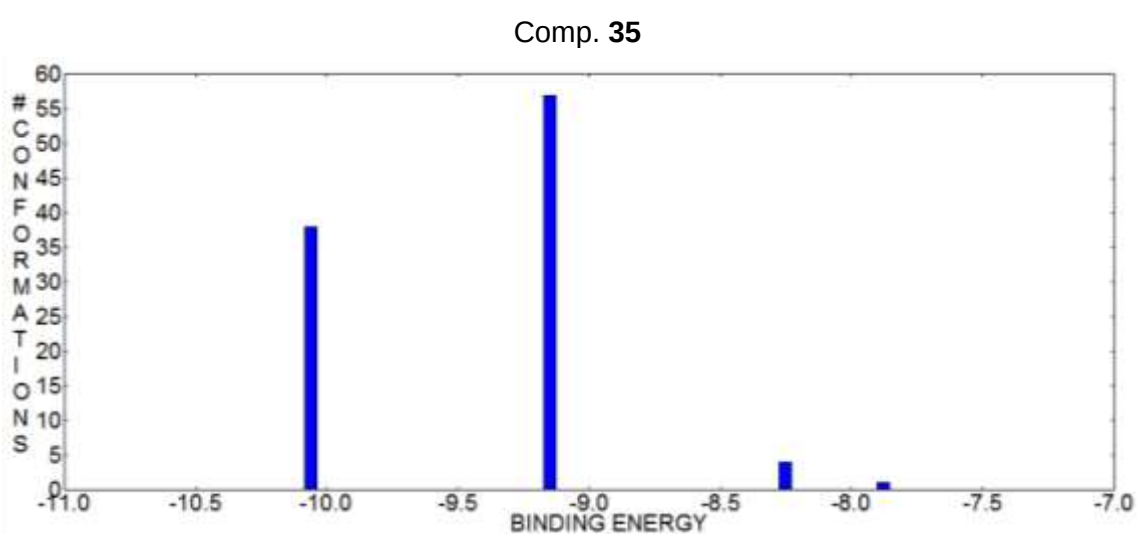

Figure S3. Docking results of compound **35** in LmjPDEB1. Two main clusters are found in the studies, containing around 95% of all potential binding modes. Cluster 1 present most favorable binding energy comparing to cluster 2

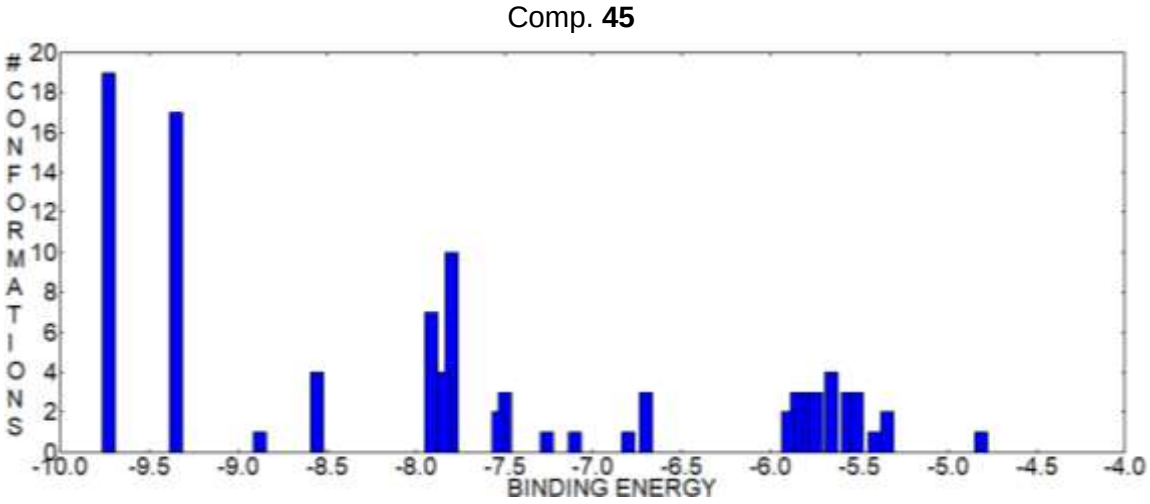

Figure S4. Docking results of compound **45** in LmjPDEB1. Several clusters are found in the studies. Cluster 1 and cluster 2 are the most populated clusters and also contains the most favorable binding poses in terms of energy. Cluster 1 was selected as the most representative one.